Design and implementation of a Zeeman slower for ^{87}Rb

Kenneth J. Günter*

Groupe Atomes Froids, Laboratoire Kastler-Brossel
Ecole Normale Supérieure, Paris

March 2004

*E-mail: Kenneth.Guenter@lkb.ens.fr, Web: www.kenneth.ch

Abstract

This article describes the design and the realization of the Zeeman slower in the frame of a new setup for the continuous-wave atom laser experiment at ENS Paris.

A beam of ^{87}Rb atoms coming out of a recirculating oven is collimated and slowed down to 20 m/s by an increasing field Zeeman slower. The resulting flux of the order of 10^{11} at/s is used to load a magneto-optical trap. After capturing in a magnetic trap, the cold atoms are injected into a magnetic guide.

Contents

1 Introduction

A spectacular challenge in the field of Bose-Einstein condensation is the achievement of a continuous beam operating in the quantum degenerate regime. This would be the matter wave equivalent of a CW monochromatic laser and it would allow for unprecedented performance in terms of focalization or collimation. In [1], a continuous source of Bose-Einstein condensed atoms was obtained by periodically replenishing a condensate held in an optical dipole trap with new condensates. This kind of technique raises the possibility of realizing a continuous atom laser. An alternative way to achieve this goal has been proposed and studied theoretically in [2]. A non-degenerate, but already slow and cold beam of particles, is injected into a magnetic guide where transverse evaporation takes place. If the elastic collision rate is large enough, an efficient evaporative cooling leads to quantum degeneracy at the exit of the guide. This scheme transposes in the space domain what is usually done in time, so that all operations leading to the condensation are performed in parallel, with the prospect of obtaining a much larger output flux.

The condition for reaching degeneracy with the latter scheme can be formulated by means of three parameters: the length ℓ of the magnetic guide on which evaporative cooling is performed, the collision rate γ at the beginning of the evaporation stage, and the mean velocity $v_{\rm b}$ of the beam of atoms. Following the analysis given in [2], one obtains

$$N_{\rm c} \equiv \frac{\gamma \ell}{v_{\rm b}} > 500 \; . \tag{1.1}$$

If the collision rate γ is constant over the cooling process, which is approximately the case for realistic conditions, this means that each remaining atom at the end of the guide has undergone $N_{\rm c}$ elastic collisions during its collisional propagation through the magnetic guide.

Some conclusions can already been drawn from the inequality (1.1). One needs to operate in a long magnetic guide, at very low mean velocity, and the collision rate should be as high as possible at the beginning of the evaporation. The criterion (1.1) can be recast in terms of the temperature T, the incoming flux ϕ, and the strength λ of the linear transverse confining potential: $N_{\rm c} \sim \phi \lambda^2 v_{\rm b}^{-2} T^{-3/2}$. We consequently need to start with a large incoming flux at low velocity and at very low temperature.

In our new experimental setup we have implemented a Zeeman slower in order to increase the initial flux. The Zeeman slower permits to slow down a beam of atoms obtained from a collimating oven. It is used to load very efficiently a huge number of atoms into a magneto-optical trap [3]. The obtained clouds are further cooled and injected into a 4.5 m long magnetic guide [4].

The following text is structured as follows: In section 2, I recall some useful theoretical results to describe the physics of the Zeeman slower. The third section is devoted to the design and simulation of the slower. Section 4 deals with the

practical implementation. Section 5 describes the atomic beam source for the Zeeman slower, a new implemented recirculating oven. In Section 6 I review the techniques to measure the atomic flux and other characteristics of the slower and present our results. Finally, the article is concluded with a summary of this work and a short outlook.

2 Theory of Zeeman tuned slowing

There are various techniques to slow and cool atomic beams [5]. Zeeman tuned slowing is the best known and is in most applications very efficient [6] and advantageous when compared with other methods like chirping [7] or broadband cooling [8, 9].

In this section I summarize the physics of the Zeeman slower. Important formulas to understand how such a slower works are introduced.

2.1 Radiation pressure

The elementary principle of cooling atoms with laser light is the momentum conservation when an atom scatters a photon. Consider a two-level atom in its ground state moving in one direction and a counter-propagating light beam with wave vector $\mathbf{k}$. By absorbing resonant photons out of the beam the atom inherits their momentum $-\hbar k$ ($k = |\mathbf{k}|$) and is decelerated. The excited atom can then spontaneously emit a photon and fall back into the ground state. Spontaneous emission again induces a momentum change of $\hbar\mathbf{k}$. However, averaged over many absorption/emission cycles it does not contribute to any deceleration of the atom since it is equiprobable in two opposite directions.

As a consequence of the spontaneous emission, the transverse velocity components of the atomic beam increase owing to transverse heating, affecting the collimation of the atom beam. This point is treated in detail in the next paragraph.

To slow a beam of ^{87}Rb atoms by an amount of $\Delta v = 350$ m/s, for instance, each of them would need to absorb $N = \frac{m\Delta v}{\hbar k} \approx 62000$ photons, where m is the mass of one atom. The dissipative force acting on the atom is derived from the optical Bloch equations and is given by

$$F = \hbar k \frac{\Gamma}{2} \frac{s}{s+1}, \tag{2.1}$$

where

$$s = \frac{I/I_0}{\Gamma^2 + \delta^2/4} \tag{2.2}$$

is the saturation parameter and Γ the natural linewidth of the transition. I/I_0 is the laser beam intensity in units of the saturation intensity, δ the detuning of the laser from the transition's resonance frequency. F is called spontaneous force and its action on the atoms radiation pressure [10].

For high light intensities and low detunings, the value of s becomes high. The maximal spontaneous force is given by the limit $s \to \infty$:

$$F_{max} = ma_{max} = \hbar k \frac{\Gamma}{2}. \tag{2.3}$$

This illustrative result states that an atom cannot absorb and subsequently emit spontaneously more than one photon every twice its lifetime, for in steady state it stays a duration of $\tau = 1/\Gamma$ in each, the ground and the excited state. Stimulated emission causes a momentum transfer to the atom of the opposite sign than for absorption and thus does not contribute to slowing.

2.2 Transverse heating of a slowed beam

As mentioned above, the random nature of the spontaneous emission leads to transverse heating when an atomic beam is slowed by a counter-propagating light beam [11]. To get a quantitative idea, we denote v_i the initial longitudinal velocity and $v_f(t)$ the final longitudinal velocity reached after a time t of the atomic beam. The number $N(t)$ of photons absorbed from the laser beam between $t = 0$ and t is

$$N(t) = \frac{v_i - v_f(t)}{v_{rec}}, \tag{2.4}$$

where $v_{rec} = \hbar k/m$ is the atom's recoil velocity. The mean square values of the transverse velocity components $v_{x,y}$ are given by

$$\langle v_{x,y}^2(t)\rangle = \alpha \frac{v_{rec}^2}{3} N(t). \tag{2.5}$$

This formula reflects the atom's random walk in velocity space due to spontaneous emission. The factor $\alpha = 9/10$ accounts for the dipole pattern. Its contribution is negligible, and we will deal with the isotropic case. It is easy to check that for the emission of one single photon one has $\langle \Delta v_x^2\rangle = v_{rec}^2/3$.

Usually $v_f \ll v_i$, and thus $v_i - v_f \approx v_i = \sqrt{9\pi k_B T/8m} \propto m^{-1/2}$ for an atomic beam emerging from an oven (see appendix A.3). On the other hand we have $v_i - v_f(t) = N(t)\hbar k/m$, and it follows that $N(t) \propto \sqrt{m}$. From eq. (2.5) we then deduce the scaling $v_{x,y} \propto m^{-3/4}$ with the atomic mass. Therefore, the problem of transverse spreading is more pronounced for lighter atoms.

We intend to calculate the mean value of the transverse displacement $x(t)$ of an atom after a time t. Each spontaneous emission event occurring at a time $t_k < t$ causes a velocity change of $(\Delta v_x)_k$:

$$x(t) = \sum_k (\Delta v_x)_k (t - t_k). \tag{2.6}$$

This sum consists of $t/\Delta t = N(t)$ terms, where Δt is the mean time between two successive events. Using $\langle t_k\rangle = t/2$, $\langle t_k^2\rangle = t^2/3$ and the fact that different events are uncorrelated, one receives

$$\langle x^2(t)\rangle = \frac{v_{rec}^2}{3}\frac{t^3}{3\Delta t} = \frac{v_{rec}^2}{3} N(t) \frac{t^2}{3}. \tag{2.7}$$

As an example, atoms slowed by an amount of $v_i - v_f = 350$ m/s over a distance of 1.1 m acquire a rms-velocity of about 85 cm/s or a rms-displacement of about 3 mm in the transverse direction. Once the atoms have reached their final velocity and are out of resonance with the decelerating light beam the effect of divergence becomes very important. For the same characteristics as above and a final velocity $v_f = 15$ m/s, the relative transverse velocity of an atom takes a non-negligible value of $\Delta v_{x,y}/v_f = 5\%$. This effect can be reduced by transverse cooling of the atomic beam, as explained later.

2.3 Doppler effect

Moving atoms see the frequency of a light wave shifted by an amount proportional to their velocity. The Doppler shift makes the spontaneous force dependent on the atoms velocity via the detuning δ which reads

$$\delta = \delta_0 - \mathbf{k} \cdot \mathbf{v}, \tag{2.8}$$

where $\delta_0 = \omega_{laser} - \omega_{atom}$ is the detuning of the laser frequency ω_{laser} from the zero-field, zero-velocity atomic resonance ω_{atom}. For a fixed δ_0 and a given laser beam intensity I, the spontaneous force will decrease during deceleration because the atom gets more and more out of resonance with the laser light due to the Doppler shift. After having absorbed $N = 2000$ photons, the effective detuning has changed by an amount $\Delta\delta = k\frac{N\hbar k}{m} = 2.5\Gamma$ away from resonance. The simplest method of slowing an atom beam, by opposing it a laser beam with frequency $\nu_{atom} = \frac{1}{2\pi}\omega_{atom}$, is thus very inefficient.

2.4 Zeeman effect

In the method of Zeeman slowing the Doppler shift of moving atoms with respect to resonance with the laser light is compensated by the energy shift due to an external magnetic field. The Zeeman Hamiltonian for an Alkali atom in an static external magnetic field $\mathbf{B}$ is obtained by minimal substitution of the momentum operator [12]. Neglecting the diamagnetic term the $\mathbf{B}$-dependent part of the Hamiltonian can be written as

$$\hat{H}_Z = (\hat{\mathbf{L}} + g\hat{\mathbf{S}})\frac{\mu_B}{\hbar}\mathbf{B} + g_I\hat{\mathbf{I}}\frac{\mu_N}{\hbar}\mathbf{B}, \tag{2.9}$$

where $g \approx 2$ (g_I) is the electronic (nuclear) gyromagnetic factor, and μ_B (μ_N) the Bohr (nuclear) magneton, respectively. The quantization axis is chosen along the direction of $\mathbf{B}$. In the case of low fields ($< 10^5$ G) and heavy atoms $\hat{H}_Z$ is much smaller than the spin-orbit interaction $\sim \hat{\mathbf{L}} \cdot \hat{\mathbf{S}}$. It can then be regarded as a perturbation to the fine structure Eigenstates $|L, S, J, M_J, I, M_I\rangle$. Here J denotes the total electronic angular momentum, I the nuclear spin and M_J and M_I their

corresponding components along the quantization axis. Consequently the Zeeman shift in the fine structure is given by the following expectation value of $\hat{H}_Z$:

$$\Delta E = \langle L, S, J, M_J, I, M_I | \hat{H}_Z | L, S, J, M_J, I, M_I \rangle = g_J \mu_B B M_J + g_I \mu_N B M_I \quad (2.10)$$

with the Landé factor $g_J = 1 + (g-1)\frac{J(J+1)+S(S+1)-L(L+1)}{2J(J+1)}$ and $B = |\mathbf{B}|$. Note that since the nuclear contribution usually is much smaller than the electronic term it can often be neglected.

An accurate calculation of the Zeeman effect in hyperfine structure requires the diagonalisation of the Hamiltonian $\hat{H} = \hat{H}_{HF} + \hat{H}_Z$ where the hyperfine interaction can approximatively be expressed as

$$\hat{H}_{HF} = \frac{A}{\hbar^2} \hat{\mathbf{I}} \cdot \hat{\mathbf{J}} = \frac{A}{2}[F(F+1) - I(I+1) - J(J+1)]. \quad (2.11)$$

Here F is the Eigenvalue of the operator $\hat{\mathbf{F}} = \hat{\mathbf{I}} + \hat{\mathbf{J}}$. For this purpose we represent the matrix of $\hat{H}$ in the hyperfine basis $|L, S, J, I, F, M_F\rangle$ where $\hat{H}_{HF}$ is diagonal. This is not the case for $\hat{H}_Z$. To obtain its matrix elements we write the basis states as linear combinations of the fine structure states with Clebsch-Gordan coefficients,

$$|I, J, F, M_F\rangle = \sum_{M_I + M_J = M_F} |I, M_I, J, M_J\rangle \langle I, M_I, J, M_J | I, J, F, M_F\rangle. \quad (2.12)$$

Here the quantum numbers L and S have been suppressed for simplicity. We then evaluate the matrix elements using (2.10). Obviously M_F (but not F) stays a good quantum number and only states with the same M_F are mixed. This fact simplifies the calculation since the diagonlisation of $\hat{H}$ is reduced to sub-Hilbert spaces identified by M_F. The resulting Eigenenergies for ^{87}Rb (nuclear spin $I = 3/2$) in the configurations $5S_{1/2}$ and $5P_{3/2}$ are plotted in Fig. 2.1.

The transition energies at a certain field B are obtained by subtracting the corresponding energy of the ground state from that of the excited state. The only closed two-level transitions, $|5S_{1/2}, F = M_F = 2\rangle \rightarrow |5P_{3/2}, F = M_F = 3\rangle$ and $|5S_{1/2}, F = -M_F = 2\rangle \rightarrow |5P_{3/2}, F = -M_F = 3\rangle$, show a linear Zeeman shift in the transition energy:

$$\Delta E_{\pm} = \pm \mu_B B, \quad (2.13)$$

where the sign stands for σ^+- or σ^--polarization of the coupling light, respectively. To include the effect of an external magnetic field $\mathbf{B}$ the detuning (2.8) is generalized to

$$\delta = \delta_0 - \boldsymbol{k} \cdot \boldsymbol{v} \mp \frac{\mu_B}{\hbar} B. \quad (2.14)$$

With a field that varies adequately along the direction of the moving atoms the Zeeman shift can compensate for the Doppler shift. That way the atoms are "pushed back" towards resonance with the decelerating laser light during their movement.

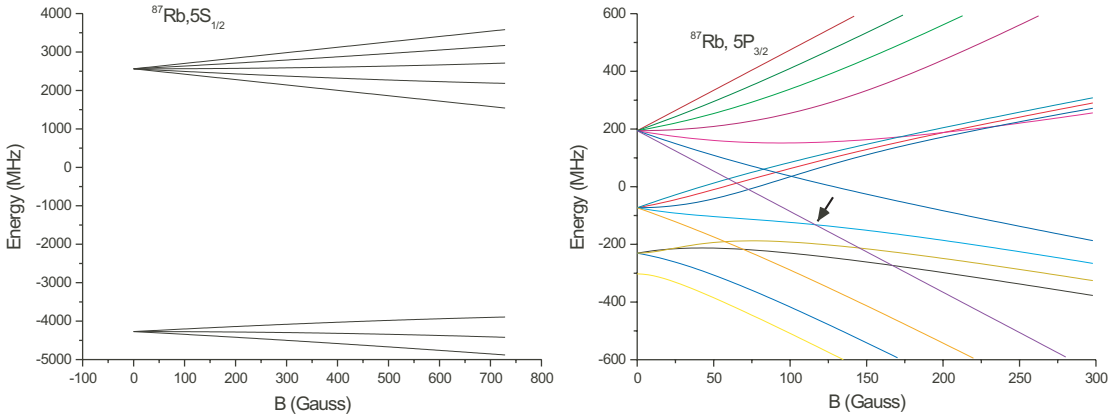

Figure 2.1: *The Zeeman splitting of the hyperfine levels of ^{87}Rb in the $5S_{1/2}$ and $5P_{3/2}$ manifolds (the nuclear magnetic moment has been neglected). The arrow indicates the crossing in the $5P_{3/2}$ manifold at about 120 Gauss where the energies of the states $|F = 2, M_F = -1\rangle$ and $|F = 3, M_F = -3\rangle$ equal.*

2.5 The magnetic field profile in a Zeeman slower

A Zeeman slower consists of a tube inside which a magnetic field is applied to shift the energy levels of the atoms moving along the axis. With the appropriate field profile atoms moving through the tube can be decelerated efficiently by a counter propagating laser beam of constant frequency. To calculate this field dependence in the slower we assume constant deceleration along the axis z of the tube, $a = const$ [13]. Setting $\delta = 0$ in eq. (2.14) (resonance condition) we have $v \propto B$. Resolving $z(t) = v_0 t + \frac{1}{2}at^2$ after the time t and substituting $t(z)$ in $v = v_0 + at$ one readily obtains a magnetic field of the form

$$B(z) = B_b \pm B_0\sqrt{1 - \frac{2az}{v_0^2}} \tag{2.15}$$

($a > 0$), where again the sign is valid for the σ^+- resp. the σ^--transition. v_0 denotes the initial velocity of the atoms (capture velocity). The external **B**-field defines a quantization axis and reduces the probability of optical depumping to non-cycling hyperfine states.

At magnetic fields where two different Zeeman levels cross each other the states are degenerated in energy. Consider for example the case of the σ^- transition. At about 120 G the cycling light may couple the $|F = 2, M_F = -2\rangle$ ground state with the $|F = 2, M_F = -1\rangle$ excited state if the polarization is not perfect (Fig. 2.1). This state lies outside the closed two-state system and can decay to

a $|F = 1\rangle$ ground state which leads to atom loss. A way around this problem consists in shifting this crossing out of the region of operation by adding to the profile constant bias field $B_b > 120$ G (see eq. (2.15)). The detuning δ_0 of the laser will be adapted to compensate for this shift. Furthermore, a repumping laser beam tuned to the transition $|5S_{1/2}, F = 1\rangle \rightarrow |5P_{3/2}, F = 2\rangle$ can be used to get atoms back which may have been optically depumped by the slowing beam. A priori it is not clear that this really helps since such a beam is not resonant with the atoms at any position in the slower (but only where the Doppler and Zeeman shifts compensate the frequency detuning of the repumping light). In practice a repumper is nevertheless useful as will be discussed in more detail in section 6.

From the corresponding sign of the Zeeman shift it is clear that $B(z)$ must decrease for the σ^+-profile in order to slow atoms and increase for the σ^--profile. The maximal velocity decrease of the atomic beam is given by the difference of magnetic field between entrance and exit of the slower. For a given field, the detuning $\Delta\nu = \delta_0/2\pi$ then determines the absolute values for the capture velocity and the final velocity of the slower. It is positive for the σ^+- and negative for the σ^--configuration. The first Zeeman slower built by Phillips and Metcalf used the σ^+-transition [14]. However, such a slower has some major disadvantage. Suppose that the atoms are decelerated to a velocity close to 0 at a finite field value. Further downstream atoms with still lower velocities will then be resonant with the laser light because of the lower field. They are slowed even more and are probable to return into the slower (negative final velocity). In an increasing field slower, on the other hand, slow atoms get quickly out of resonance after they have passed the maximum magnetic field at the end. The final velocity is well defined and limited by the peak value of B. As a result, a σ^--slower loads a MOT much more efficiently, for instance. Furthermore, it is less sensitive to fluctuations in laser frequency and intensity than a σ^+-slower [15].

It is clear that the magnetic field profile must not be designed for a value of $a > a_{max}$ (compare eq. (2.3)). Otherwise the atoms will not follow the desired deceleration determined by the slope of the field. This imposes a criterium on the steepness of the field (2.15) along the slower axis [13]. Using eq. (2.14) we have

$$a = \frac{dv}{dt} = v\frac{dv}{dz} = \pm\frac{\mu_B v}{\hbar k}\frac{dB(z)}{dz}, \tag{2.16}$$

and $|a| \leq a_{max}$ leads with $\lambda = 2\pi/k$ and $h = 2\pi\hbar$ to the condition

$$\left|\frac{dB(z)}{dz}\right| < \frac{\hbar k a_{max}}{\mu_B v} = \frac{h a_{max}}{\mu_B \lambda v}. \tag{2.17}$$

In practice one usually works with $a \approx \frac{2}{3}a_{max}$. The criterium determines the minimal required length of the slower. For example, a Zeeman slower which decelerates ^{87}Rb atoms from 400 m/s to 0 m/s needs to be at least $l = \frac{\Delta v^2}{2a_{max}} = \frac{m\Delta v^2}{\hbar k\Gamma} = 75$ cm long. Obviously, heavier atoms with longer lived excited state are harder to

decelerate. Of course, the required capture velocity is lower for heavier atoms, though.

An important feature of the Zeeman slower is that the initial velocity distribution of the atoms is narrowed when they are decelerated. Because the resonance condition for slower atoms is fulfilled at a later position in the slower, all atoms are bunched into the same slow velocity group. It is this compression of the velocity distribution in phase space which makes the difference between cooling and slowing.

3 Design and simulation of the slower

Our Zeeman slower was implemented in the σ^--configuration and produces, beside the tapered field, a bias field of 250 G.

The magnetic field in a Zeeman slower is produced by a solenoid. In the process of designing the slower a computer simulation was programmed which serves mainly two purposes. First, we determined the currents in the solenoid wire necessary to generate the desired magnetic field profile, and second, we simulated the motion of the atoms in this slower profile.

3.1 Calculation of the magnetic field

To compute the magnetic field we modelled the coils if the solenoid as cylindrical layers of a given length, each carrying a homogeneous current density. Their thickness corresponds to the diameter of the wire which is used to wind the tube. The bias field is realized by current layers over the entire length of the slower. The coils to generate the tapered field are laid above these layers.

The magnetic field at a space point $\mathbf{x}$ produced by a static current density distribution $\mathbf{j}(\mathbf{x}')$ is given by the law of Biot-Savart [16]:

$$\mathbf{B}(\mathbf{x}) = \frac{\mu_\mathbf{0}}{\mathbf{4}\pi} \int \mathbf{j}(\mathbf{x}') \times \frac{\mathbf{x}-\mathbf{x}'}{|\mathbf{x}-\mathbf{x}'|^\mathbf{3}} d^\mathbf{3}\mathbf{x}' \tag{3.1}$$

(SI units, μ_0 induction constant). The diameter of the wires is much smaller than the diameter of the slower tube, so that the winding helicity of the coils can be neglected. Using the notation $\mathbf{x}' = (x', y', z')$ and the variables $r' = \sqrt{x'^2 + y'^2}$ and $\varphi' = arg(y'/x')$, the current density of a cylindrical layer with radius r_0 from z_1 to z_2 can then be written as

$$\mathbf{j}(\mathbf{x}') = j_0 \begin{pmatrix} -\sin\varphi' \\ \cos\varphi' \\ 0 \end{pmatrix} \delta(r'-r_0) f(z'; z_1, z_2) \tag{3.2}$$

$$\text{with } f(z'; z_1, z_2) = \begin{cases} 1 & z_1 \le z' \le z_2 \\ 0 & \text{else} \end{cases} .$$

Inserting this into eq. (3.1) and setting $r = 0$ we get the magnetic field of a layer on the axis of the tube:

$$\boldsymbol{B}(r=0,z) = \frac{\mu_0}{2} j_0 \hat{\boldsymbol{u}}_z \int_{z_1}^{z_2} \frac{r_0^2}{[r_0^2 + (z-z')^2]^{3/2}} dz' = \frac{\mu_0}{2} j_0 \hat{\boldsymbol{u}}_z \frac{z-z'}{\sqrt{r_0^2 + (z-z')^2}} \Bigg|_{z'=z_2}^{z'=z_1} . \tag{3.3}$$

$\hat{\boldsymbol{u}}_z$ is the unit vector in the z-direction.

Off-axis the magnetic field has also a radial component and its absolute value is higher. Note that the calculation of these fields involves elliptic integrals and cannot be simply evaluated analytically. The total magnetic field is obtained by summing over all the layers.

3.2 Current configuration for the solenoid

Since it is desirable to use the same power supply for the all the layers — except for the bias coils which need a higher current — we defined a fixed current density. In order to get a smooth increasing field, each layer in the design was basically divided into three parts. With increasing z, we assigned the quarter of the current density to the first part, half of it to the second part and its full value to the last one. We would then just wind the coils with the corresponding spacing between two loops to be able to use one single wire. This scheme is illustrated in Fig. 3.1. The positions and currents of the layers are adjusted to fit as precisely as possible the curve described by eq. (2.15). The final design of the solenoid consisted of two bias field layers and 13 layers.

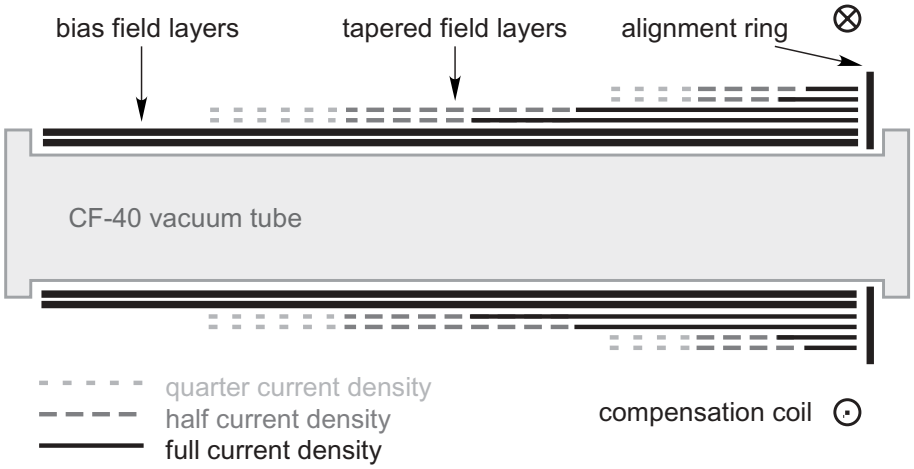

Figure 3.1: *Scheme for the current densities in the coil layers of the Zeeman slower.*

At the end of the slower an additional coil is mounted with the purpose of compensating the magnetic field and its gradient in the MOT region of our experimental setup, 14 cm away from the end of the slower. Apart from that, the compensation coil also helps the field to fall off quickly at the end. In our experimental setup the Zeeman slower is mounted perpendicular to the magnetic guide for optimal loading of the elongated magneto-optical trap. We noticed that in this configuration the MOT was hardly by the magnetic field produced by the Zeeman slower.

The field profile of our solenoid and its deviations from the ideal curve are plotted in Fig. 4.1 and 4.2. To get an idea of the quality of the magnetic field profile we allowed an error of $1 \cdot \frac{h}{\mu_B}$ MHz from the theoretical curve with the laser intensity of the unfocused beam. Towards the beginning of the slower the increasing light intensity of the focused beam (see below) can compensate partially for any deviations in the magnetic field (eq. (2.2)). Fig. 4.2 also shows the allowable error range for the magnetic field when we want to keep the saturation parameter constant. The field values are within the margin along the entire profile.

3.3 Simulation of the atoms' motion

A first test for the designed field profile consisted in the simulation of the atom's movement inside the Zeeman slower. For this purpose the equation of motion (2.1) was numerically solved, where $B(z)$ specified the detuning δ (eq. (2.14)) in the saturation parameter given by eq. (2.2).

The slowing laser beam had an initial size of 3 cm diameter at the end of the slower and was focused to 1.5 m away [17]. This provides some transverse cooling for the atoms and reduces the divergence of the atomic beam [10, 11]. To include this effect in the simulation, the light intensity was set to

$$I = I_0 exp\left(-\frac{2r^2}{\omega_0^2\left[1+\left(\frac{\lambda z}{\pi w_0^2}\right)^2\right]}\right)\left(\frac{1.5\text{ m}}{z}\right)^2, \tag{3.4}$$

where ω_0 is such that at $z = 1.5$ m the beam size is 3 cm (origin of z-axis at slower entrance and z increasing towards slower end). We designed the magnetic field profile for a deceleration $a \approx \frac{2}{3}a_{max}$ which requires a laser beam intensity $I/I_0 = 2.6$ (compare eq. (2.2)). Setting the laser detuning $\delta_0 = -2\pi \cdot 630$ G we adjusted the capture velocity of the atoms to about 380 m/s. The end velocity is then determined by the difference in the magnetic field between the end and the beginning of the slower. In our design this value was 340 Gauss, leading to an end velocity of about 20 m/s.

Fig. 3.2 shows the atoms' velocity $v(z)$ and the actual detuning $\delta(z)$ in function of their position z. This data was obtained using the real (experimental) magnetic field produced by the solenoid (see section 4) in the simulation. If the criterium (2.17) was not fulfilled at some point, one would see a breakthrough in the plots. The atom would not be decelerated any longer and the detuning would suddenly rise because the atoms could not follow the magnetic field. Too low light intensity has the same effect.

To estimate the influence of the higher magnetic field and lower laser intensity off-axis we also simulated the atoms' motion 15 mm away from the center of the

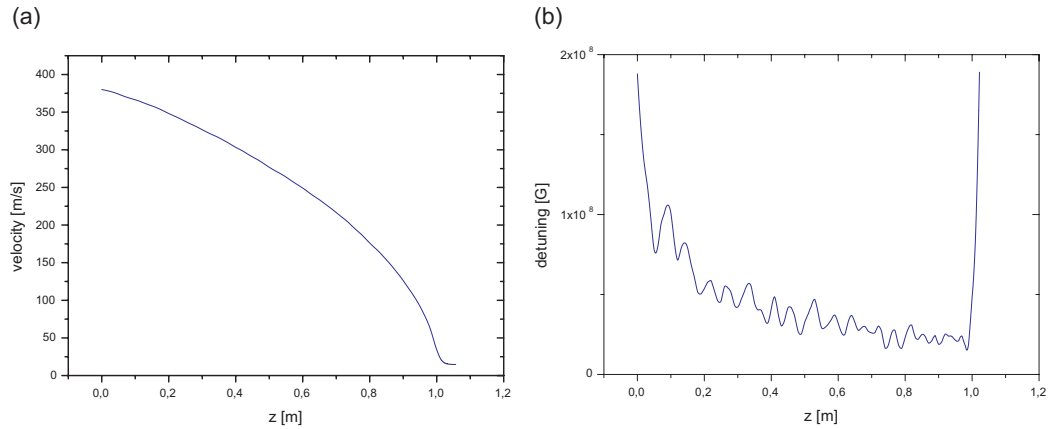

Figure 3.2: *Simulation using the final experimental* **B** *field produced by the slower. (a) Evolution of the atoms velocity along the slower. (b) The laser's detuning from the actual atomic resonance along the slower.*

tube. With the same parameters as above the atoms were still decelerated without any breakthrough to a final velocity only a few m/s lower than on-axis.

3.4 Characteristics of the designed slower

We give a summary of the parameters and characteristics of the simulated Zeeman slower:

length	1.1 m
bias field (initial field)	250 G
final magnetic field	590 G
laser detuning	-880 MHz
laser intensity	2.6 I/I_0
beam waist	30 mm
capture velocity	380 m/s
end velocity	20 m/s

Please note that some of these designed characteristics differ from the definitive values of the actual slower. The corresponding experimental data is given in section 6.

4 Building the slower

This section describes the practical realization of the Zeeman slower and gives an overview of the used material.

4.1 The vacuum tube and the wire

A 1.20 m long CF-40 vacuum tube was used to integrate the slower in our vacuum system. The inner diameter of 38 mm allows the use of a slowing beam with a sufficiently large waist. The efficient magnetic field profile extends over a length of 1.1 m which is longer than the minimal requirement (see section 2). This allows the field to be less steep which makes the slower less sensitive to field deviations, or — in the perfect case — to increase the capture range. Before winding the solenoid an electrically isolating spray was applied along the entire vacuum tube to avoid electric contact to any un-isolated parts of the current carrying wire.

To build the coils producing the bias field a copper tube wire with an inner (outer) diameter of 3 (4) mm was used. This allows water cooling the coils which would heat up remarkably with the amount of current we let pass. Since we wanted to implement a bakable Zeeman slower the tube wire was isolated with high temperature teflon heat shrink sleeves (Pro Power multicomp STFE4 6.4 CLR). The specified shrink factor of 4 was a bit too high for our purpose, so slow and uniform heating in an oven was necessary in order to make the sleeves shrink the right amount (i.e. the temperature in the oven was increased with a rate of 1 °C/min).

The coil layers for the tapered field were wound with standard capton-isolated (bakable) copper wire of a diameter of 1.8 mm. Using wire with a squared cross section would have been advantageous. It prevents the wire loops from slipping between the larger copper tubes of the bias layer below. The winding would be more homogeneous and accurate. This type of wire, however, was not easy to obtain at the time yet.

4.2 Winding the coils

A turning lathe in our workshop facilitated the winding of the coils. The clamped CF-40 tube could be wound just by holding the wire tight while it was turning. An aluminium plate perpendicular to the tube was mounted at its end to align the wires at the end of the layers. The two layers for the bias field were built with separate tube wires to be able to cool them in parallel. The current circuit, however, was in series. At both ends the coils were provisionally fixed with collars which were separated from the layers by a teflon band. Finally, the bias field coils were covered with a 0.2 mm thick copper sheet, fixed with epoxy to provide an even ground to wind the remaining coils consisting of thinner wire.

radius [mm]	positions of layers with quarter, *half* and **full** current density [mm]					
28.9	,	,	*190*, *239*	**239**, **265**	*265*, *304*	**304**, **1143**
30.7	370, 393	412, 491	*491*, *504*	**504**, **521**	*521*, *545*	**545**, **1143**
32.5	370, 393	,	,	412, 491	491, 637	**637**, **1143**
34.3	,	,	,	674, 741	*741*, *800*	**800**, **1143**
36.1	,	,	,	674, 741	*741*, *861*	**861**, **1143**
37.9	,	,	,	881, 919	*919*, *956*	**956**, **1143**
39.7	,	,	,	881, 919	*919*, *998*	**998**, **1143**
41.5	,	,	,	,	*1030*, *1067*	**1067**, **1143**
43.3	,	,	,	,	*1030*, *1067*	**1067**, **1143**
45.1	,	,	,	,	,	**1073**, **1143**
46.9	,	,	,	,	,	**1073**, **1143**
48.7	,	,	,	,	,	**1077**, **1143**
50.5	,	,	,	,	,	**1077**, **1143**

Table 4.1: *Loop radii and (start, end) positions of the coil layers (only bias field corrected), measured from the outer side of the entrance flange.*

Table 4.2 shows the data of the coils producing the tapered magnetic field. To wind the layers with half of the nominal current density a second wire was wound at the same time, keeping the correct spacing between the current carrying loops. All layers consist of one single piece of wire. Therefore the winding helicity of a coil would be opposite to the one of the layer underneath it. At some places the wire would then slip into the gap between two wires below, resulting in an irregular and totally reduced loop density. By adjusting the remaining layers in the simulation appropriately we could correct these errors. Finally, another series of correction loops was added after measuring the total field produced as described below. The positions and current densities of the those layers are summarized in table 4.2. The thin wire was provisionally fixed with cable ties which later were replaced by wire straps. A way around the irregular slipping problem would be to use wire with a squared cross section.

radius [mm]	positions of layers with **full** and third current density [mm]			
28.9	**125**, **150**	**25**, **75**	,	,
30.7	**230**, **239**	**283**, **298**	,	,
34.3	**375**, **385**	**455**, **475**	**530**, **541**	605, 655
37.9	**715**, **720**	**790**, **800**	**832**, **845**	,
41.5	**893**, **910**	**953**, **970**	1005, 1035	,
45.1	**1035**, **1050**	,	,	,

Table 4.2: *Loop radii and (start, end) positions of the additional correction layers, measured from the outer side of the entrance flange.*

The magnetic field produced by the solenoid was measured using a Hall probe. For this purpose the following currents were supplied: 41 A for the bias coils, 4 A for the tapered field coils and 37 A for the compensation coil. The results are plotted in Fig. 4.1. Fig. 4.2 shows the deviations from the theoretical field profile.

4.3 The cold finger

At the slower entrance a cylindrical copper piece acting as a cold finger is concentrically mounted inside the vacuum tube to provide further pumping. Transversally moving Rubidium atoms which hit the cylinder remain stuck to its walls. Cooling the cylinder to -20 °C is accomplished from outside the vacuum by thermal conduction of a ceramic-insulated feed-through piece (usually used for electric current). Connected to it is a copper block cooled by two 60 W Peltier elements in series. Heating of the opposite sides of the Peltier elements is limited by the contact with another, water cooled, copper block.

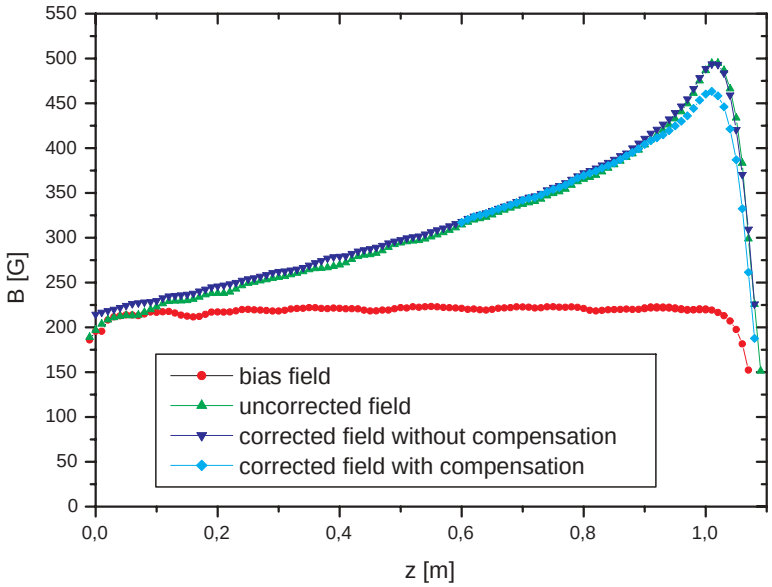

Figure 4.1: *Measured magnetic fields of the Zeeman slower before and after corrections.*

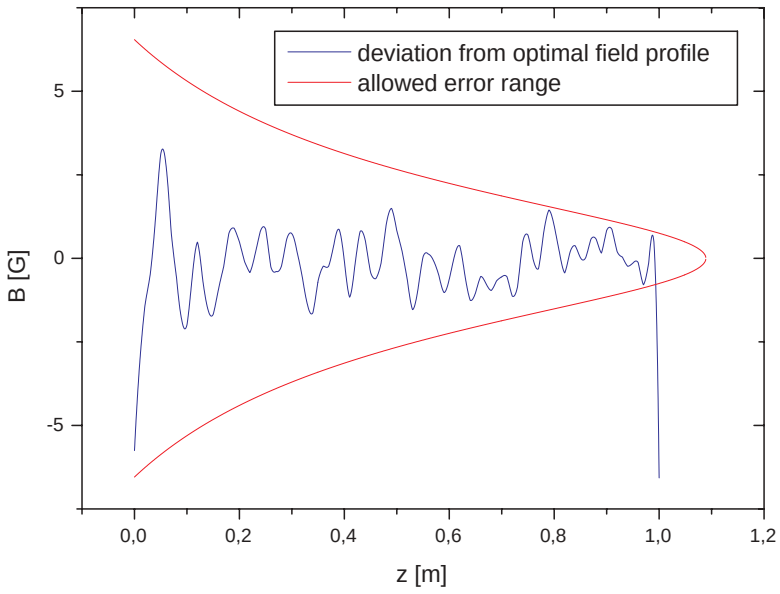

Figure 4.2: *Deviations of the measured magnetic field from the theoretical profile. The errors are within the range as discussed in section 3.*

5 The (recirculating) Rubidium oven

With the implementation of a Zeeman slower in our experimental setup we also introduced a new Rubidium source to provide a high load of atoms. This section describes the recirculating oven which replaces the former room temperature gas chamber. To get more insight into the subject of atomic beam sources, please consult the references [18] and [19].

5.1 The setup

The atom beam source consists mainly of three different chambers as shown in Fig. 5.1. The first one is the oven containing the Rubidium source at its bottom. It is heated at four different points to produce the desired vapor pressure and particle flux. The atoms leave the oven through an aperture A_1 (4 mm diameter) and enter the second chamber. They are then collimated by a second aperture A_2 (7.8 mm diameter) to form a beam. The third chamber is terminated by another aperture A_3 (8.5 mm diameter) which improves the collimation. Atoms with high transverse velocities are stuck in the second chamber. Its walls are covered with a gold coated stainless steel mesh which gets wetted by the Rubidium. Our hope is that these "lost" atoms are recirculated by a tube leading back to the bottom of the oven which should increase the oven's lifetime considerably.

Rubidium has a melting point of 38.9 °C and is highly reactive, in particular with oxygen. Before putting the Rubidium the oven was vented with hydrogen in order not to contaminate it with air. To fill the oven chamber with Rubidium we cooled the ampuls in liquid Nitrogen before breaking them up on one side and put them upside down into the oven tube. This prevents any violent reactions with oxygen contained in the air. One usually fills 10 to 20 g (one or two ampuls). When heating up, the Rubidium becomes liquid and drops to the bottom of the oven while the empty ampuls remain in the upper part of the tube (Fig. 5.1).

5.2 Expected performance of the atom beam source

The vapor pressure for Rubidium at a given temperature T in the oven chamber is given by the following Antoine equation [20]:

$$\log_{10} P_{sat}[\mathrm{Pa}] = 9.318 - \frac{4040}{T[\mathrm{K}]}^{*}. \tag{5.1}$$

For an ideal gas the particle density n is determined with

$$P_{sat} = n k_B T. \tag{5.2}$$

*The Antoine equation is an empirical extension to the Clausius-Clapeyron equation $T\frac{dP_{sat}}{dT} = \frac{l}{\Delta v} \approx \frac{l}{v_{gas}}$, where l and $\Delta v = v_{gas} - v_{fluid}$ are the latent heat and the volume difference.

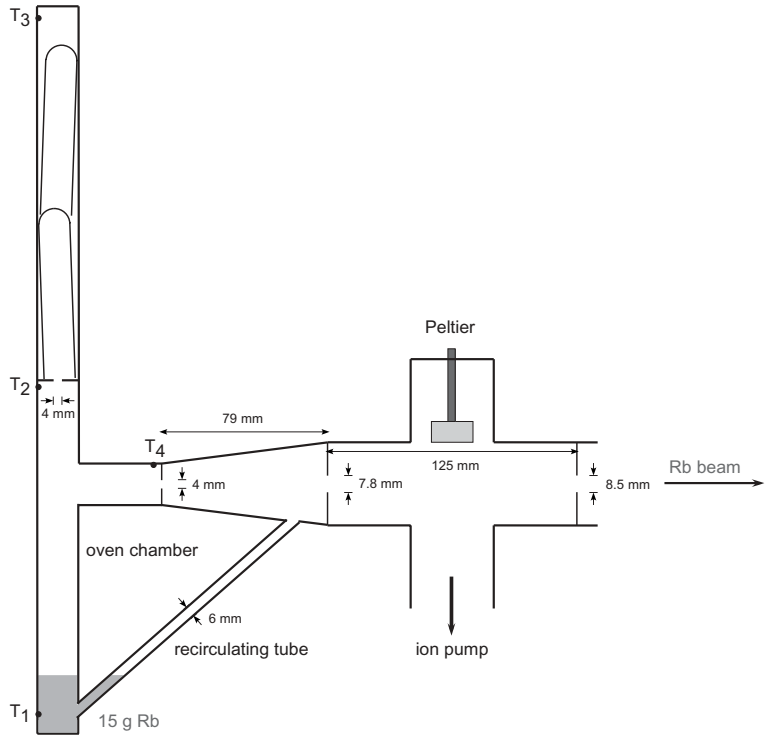

Figure 5.1: *The atomic beam source, consisting of a recirculating oven and collimators, and its dimensions. The Peltier element serves as an additional Rb pump.*

To illustrate the importance of the recirculation we compare the particle flux out of the oven chamber with the one after the collimation. The derivation of these quantities is done in appendix A. The results are as follows (notation as in Fig. 5.1):

$$\Phi_0 = \frac{1}{4} n A_1 \bar{v}, \tag{5.3}$$

the flux out of the oven chamber, and

$$\Phi_c = \frac{n A_1 A_3 \bar{v}}{4\pi d^2}, \tag{5.4}$$

the flux of the collimated beam. Both depend directly on the oven temperature through $\bar{v} = (\frac{8k_B T}{\pi m})^{1/2}$. In our setup the distance between A_1 and A_3 is $d = 20.4$ cm, so the atomic beam only contains $\Phi_c/\Phi_0 = A_3/\pi d^2 \approx 0.2\%$ of the atoms that leave the oven. In other words, recirculation can in principle increase the oven's lifetime by a factor 500.

Pressure, density and flux for rubidium in function of T

Temperature [C]	Pressure [Pa]	Pressure[Torr]	Density [m-3]	Beam velocity [m/s]	Flux of ^{87}Rb [at/s]	Lifetime of 1g [h]
100	3,10E-02	2,33E-04	6,02E+18	356	8,17E+11	338
110	5,94E-02	4,47E-04	1,12E+19	360	1,55E+12	179
120	1,10E-01	8,28E-04	2,03E+19	365	2,83E+12	98
130	1,98E-01	1,49E-03	3,56E+19	370	5,03E+12	55
140	3,46E-01	2,60E-03	6,07E+19	374	8,68E+12	32
150	5,90E-01	4,43E-03	1,01E+20	379	1,46E+13	19
160	9,79E-01	7,36E-03	1,64E+20	383	2,40E+13	12
170	1,59E+00	1,20E-02	2,60E+20	387	3,85E+13	7
180	2,53E+00	1,90E-02	4,04E+20	392	6,05E+13	5
190	3,94E+00	2,96E-02	6,16E+20	396	9,32E+13	3
200	6,02E+00	4,53E-02	9,22E+20	400	1,41E+14	2
210	9,04E+00	6,80E-02	1,36E+21	405	2,09E+14	1
220	1,34E+01	1,00E-01	1,96E+21	409	3,06E+14	1
230	1,94E+01	1,46E-01	2,80E+21	413	4,41E+14	1
240	2,79E+01	2,10E-01	3,93E+21	417	6,27E+14	0
250	3,94E+01	2,96E-01	5,46E+21	421	8,77E+14	0
260	5,50E+01	4,14E-01	7,48E+21	425	1,21E+15	0
270	7,58E+01	5,70E-01	1,01E+22	429	1,66E+15	0
280	1,03E+02	7,77E-01	1,35E+22	433	2,24E+15	0
290	1,39E+02	1,05E+00	1,79E+22	437	2,99E+15	0
300	1,86E+02	1,40E+00	2,35E+22	441	3,95E+15	0

Table 5.1: *Calculated data for our Rubidium source(^{85}Rb and ^{87}Rb). The flux after collimation is given. Note that the indicated oven lifetime is valid for a* non-recirculating *oven.*

5.3 Temperature control

From eq. (5.2) and (5.3) we deduce $\Phi \sim \frac{P_{sat}}{T}$. Table 5.1 lists oven pressure, density, velocity, flux and lifetime in function of the temperature. While a conventional oven at usual operating condition has a lifetime of about 800 hours, our oven — if it recirculates — is expected to operate for at least one year without refilling of Rubidium.

To control the atomic flux out of our oven, we use four heating tapes, thermocouplers and PID temperature controllers (Omega CN1166-DC1). Thermal isolation is improved by a fiber glass cord wound around the oven chamber. The oven temperature T_1 is typically kept between 120 and 160 °C, whereas the remaining three heating points T_2, T_3 and T_4 are 30 °C above the value of T_1 (Fig. 5.1). This prevents the Rubidium from sticking to the oven walls.

6 Testing and characterization

In the following paragraphs I describe our experimental setup to test and characterize the Zeeman slower and present the results of our measurements.

6.1 Setup and Probing

The recirculating Rb oven described in the previous section served as our atomic beam source for our slower. For the measurements presented here the oven temperature was set to $T_1 = 160$ °C. This corresponds to a mean velocity of $\bar{v}_z^{jet} = (9\pi k_B T/8m)^{1/2} = 380$ m/s and a mean velocity spread of $\Delta v_z^{jet} = 145$ m/s (see Appendix A.3). T_2, T_3 and T_4 were kept at 190 °C. Our vacuum system had a pressure of 10^{-8} Torr at the time of the measurements. It must be mentioned that we still had not baked out the slower tube at this point. This way we could leave the provisional (un-bakable) cable ties which fixed the wire on the tube and eventually move the wire loops for any corrections.

The coils of the Zeeman slower are powered as follows: bias field coils 49 A, tapered field coils 5 A and compensation coil 42 A.

All our light sources consist of diode lasers. The frequency of the slowing beam is detuned by an amount of $\delta_0 = -880$ MHz to the cycling transition by means of acousto-optical modulators (AOMs). For the repumper we choose a detuning of -115 MHz, a value which is determined experimentally by optimizing the loading rate of the magneto-optical trap. Only the slowing laser is frequency-locked using RF modulation spectroscopy [21]. Slowing and repumping light are mixed and injected into a tapered amplifier (Toptica TA 100) to enhance the power. In principle we were able to get 400 mW out of the TA. However, it resulted that in this case the repumping light was hardly amplified and contributed only as a tiny fraction to the total output power. We finally ended up with an output of totally 170 mW which is fed into a glass fiber and σ^--polarized. At the 14-way-cross vacuum chamber, where the beam enters the slower, it has a maximal intensity of 9 mW/cm^2 corresponding to $5I_0$ and a profile with a $1/e^2$- diameter of 20 mm.

We detect the atoms at the exit of the Zeeman slower by measuring the absorption of weak a probing laser beam whose frequency is scanned over the transition of interest. With probe beams perpendicular and an angle of 45° to the slower axis we are able to obtain Doppler free absorption spectra as well as information about the axial velocity distribution.

6.2 Determination of the atomic flux

An incident light beam of intensity I_{in} suffers absorption by atoms. We assume this beam to be weak in intensity ($I \ll I_0$) so that the atoms' absorption does not

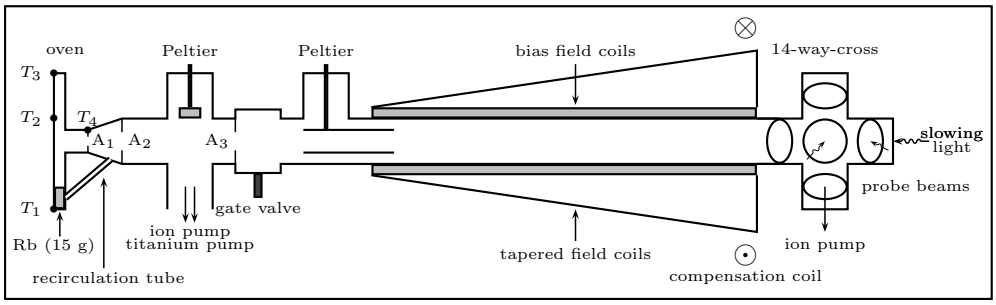

Figure 6.1: *Experimental setup to test the Zeeman slower. The slowed atoms are probed in a 14-way-cross vacuum chamber which will later serve as a chamber for the 2D-MOT.*

saturate. The transmitted intensity I_{tr} is then given by

$$I_{tr} = I_{in}\hat{T} = I_{in}e^{-\int_{-\infty}^{\infty} n(x)\sigma dx}, \tag{6.1}$$

where $n(x)$ is the particle density per unit volume at a location x and σ the cross section. The integral is to be taken along the path of the laser beam. The optical density is defined as the negative exponent of the transmission coefficient $\hat{T}$:

$$D = -\log\hat{T} = \int_{-\infty}^{\infty} n(x)\sigma dx \approx n\sigma l. \tag{6.2}$$

The approximation is valid when the density n does not vary a lot over the distance l where the beam interacts with the atoms. The flux of an atomic beam with mean velocity v reads

$$\Phi = n\frac{\pi l^2}{4}v = \frac{\pi l}{4\sigma}Dv. \tag{6.3}$$

The cross section for scattering resonant light of wavelength λ is given by $\sigma \approx \lambda^2/2\pi$ (cycling transition, linear polarization). By measuring the absorption one can calculate the optical density and determine the atomic flux. Absorption peaks of a gas usually show various enlargement effects, as Doppler or power broadening, which have to be taken into account. Given that the number of detected atoms is not changed, the surface below the absorption peak with or without broadening effects is the same. Thus, as an approximation the ratio of the height of the unbroadened absorption peak to the broadened one is the inverse of the ratio of their full widths of half maximum, $\Delta\nu/\Gamma$ with $\Gamma = 5.9$ MHz.

The absorption profile obtained with the 45° probe is plotted in Fig. 6.2. We measured an absorption of $1 - \hat{T} = 1.27\%$ at a frequency shifted by $\Delta\nu_{45°} = 20$ MHz with respect to the Doppler free spectrum. The velocity of the slowed beam is given by $v = \lambda\Delta\nu_{45°}/\cos 45° = 22$ m/s. This corresponds to an atomic flux of

$$\Phi = 1.8 \cdot 10^{11}\text{at/s} \tag{6.4}$$

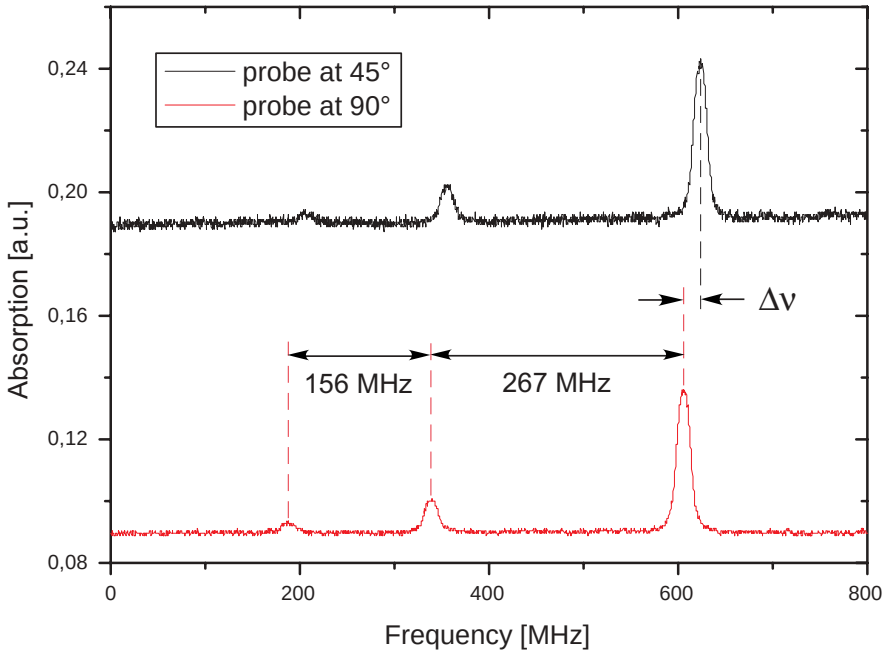

Figure 6.2: *Typical absorption spectra of the atoms coming out of the slower. The three transitions from $|F = 2\rangle$ to $|F' = 1\rangle$, $|F' = 2\rangle$ and $|F' = 3\rangle$ can be identified. The atoms' velocity is determined by the frequency difference between two corresponding peaks.*

at the exit of the Zeeman slower ($l = 3$ cm). The total broadening of the absorption peak of 17 MHz gives us an upper limit for the slow atoms' velocity spread: $\Delta v <$ 19 m/s.

Reducing the bias field over a quite wide range does not affect the flux. This is not surprising since our usual bias field value of 250 G is much higher than the field of 120 G where the critical level crossing is situated (see paragraph 2.5). After a fine adjustment of the parameters and alignment of the slowing beam we were able to obtain a flux of about $5 \cdot 10^{11}$ at/s (5% absorption, $T_1 = 140$ °C, $v = 16$ m/s) in a later measurement.

6.3 Temperature and light dependency

We measure the flux out of the slower in function of the oven temperature and of the slowing light intensity. The results are plotted in Fig. 6.3 and 6.5.

By probing the atomic beam at 90° with the decelerating laser beam off we are able to measure the total flux (including un-slowed atoms). The ratio between the total and the slowed flux corresponds to the capture efficiency. In Fig. 6.4 this quantity is plotted in dependance of the oven temperature. As expected, for

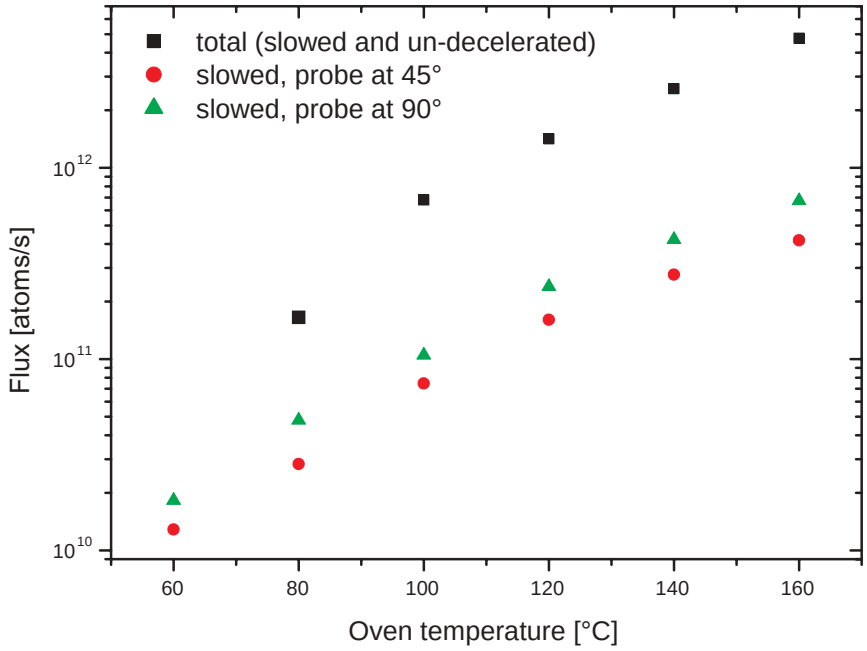

Figure 6.3: *Measured fluxes in function of the oven temperature.*

high temperatures the capture efficiency decreases slightly because of the changing velocity distribution of the atoms. According to eq. (A.10) of the appendix the portion of atoms with a velocity below the capture velocity of the slower is calculated as:

$$p_{capt} = \frac{\int_0^{v_{capt}} dv_z v_z^3 \exp(-\frac{mv_z^2}{2k_BT})}{\int_0^{\infty} dv_z v_z^3 \exp(-\frac{mv_z^2}{2k_BT})}. \tag{6.5}$$

For $v_{capt} = 380$ m/s this quantity varies between 66% and 52% for an oven temperature between 60 °C and 160 °C. The measured capture efficiency as plotted in Fig. 6.4 varies slowly around a value of 13%. This result is quite satisfying considering the additional atom loss due to transverse heating (see paragraph 2.2). Slight changes in the polarization of the slowing beam did not show remarkable effects. Also, the slower works well without repumping light (see section 2), although it helps as one sees when optimizing its frequency detuning for the MOT loading.

6.4 Final velocity of the slowed atoms

The slowing laser beam is detuned from the atomic resonance by means of an acousto-optical modulator (AOM). The frequency offset is adjusted by changing the voltage of the voltage-controlled oscillator (VCO) which drives the AOM

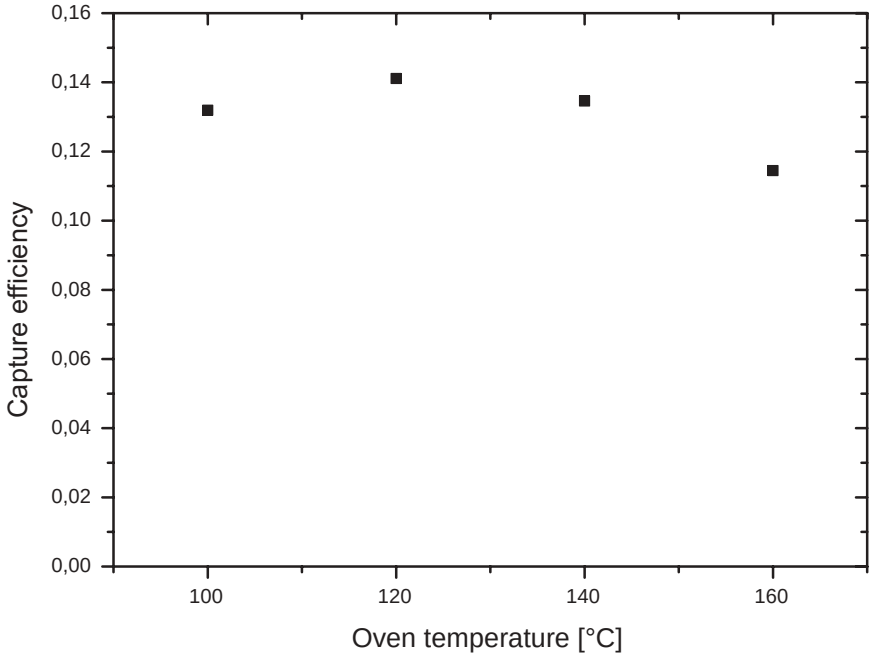

Figure 6.4: *The capture efficiency of the Zeeman slower in function of the oven temperature.*

through an RF-amplifier. Fig. 6.6 shows the measured mean velocity of the atoms leaving the slower as a function of the detuning. The continuous line represents a linear fit with free parameters to the experimental data points. The dashed line is a fit with a slope fixed at the theoretical value of $\lambda = 0.78$ m/s/MHz. The steeper than expected slope seems to fit well for lower velocities which could be due to off-resonant scattering. Slow atoms at the end of the Zeeman slower are more affected since they stay close to resonance for a longer time.

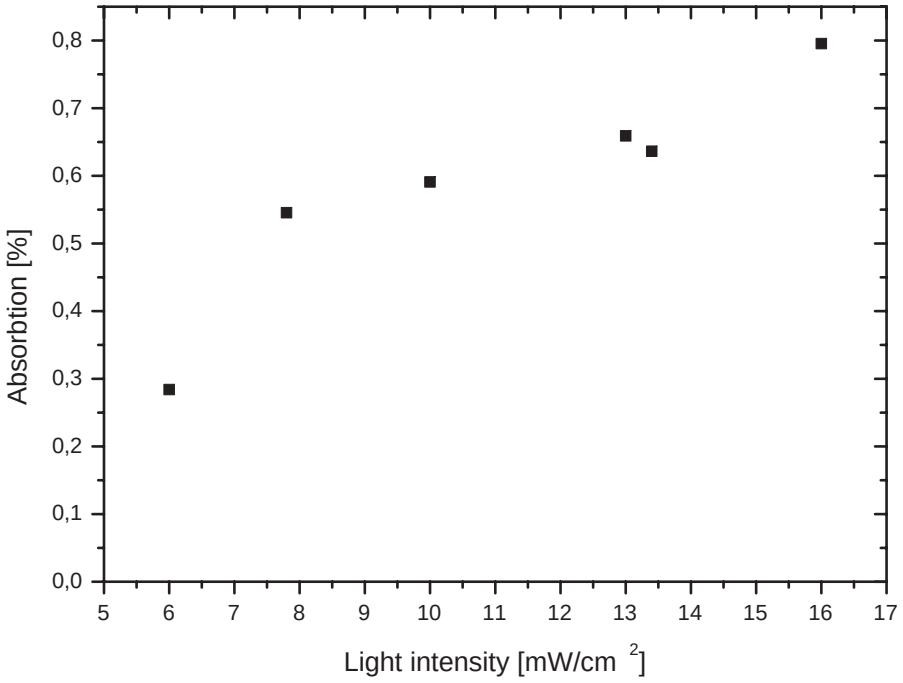

Figure 6.5: *Measured flux in function of the slowing beam intensity. Please note that this data was obtained with a configuration which differs from the current one: The repumping light was not amplified in the MOPA together with the cycling light at the time yet.*

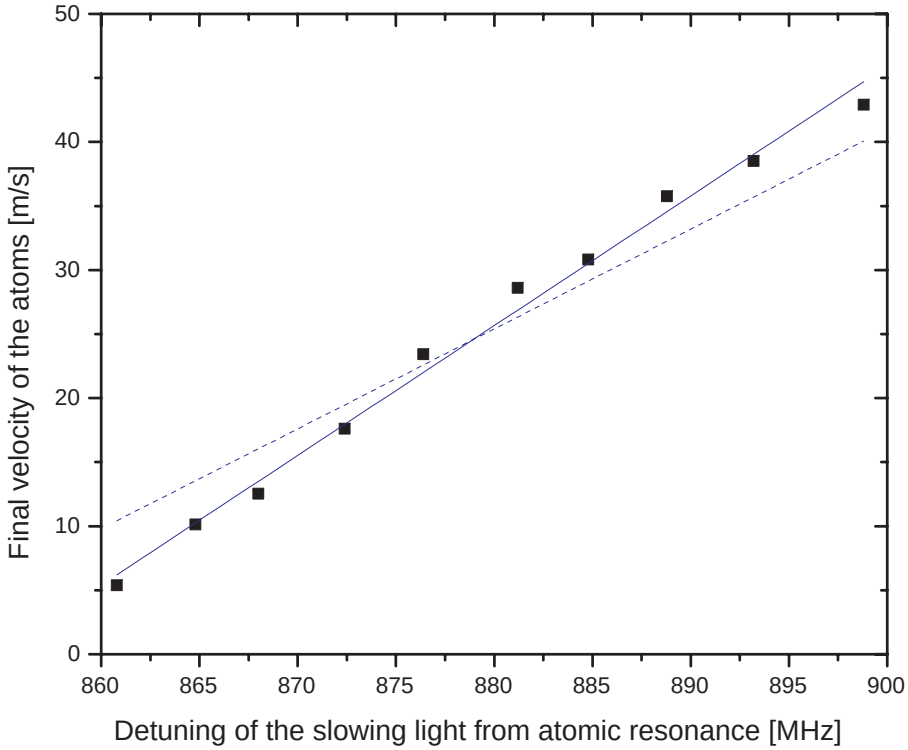

Figure 6.6: *Final velocity of the slowed atomic beam as a function of the detuning of the slowing light from the atomic resonance. The dots represent the experimental data, the lines are linear fits. For the dashed line the slope was fixed at* $\lambda = 0.78$ *m/s/MHz.*

7 Summary and Conclusions

In this article I have described the theory, design and building of a Zeeman slower for ^{87}Rb.

The implemented increasing field slower shows excellent performance. It provides a flux of the order of 10^{11} at/s at a final velocity of the order of 10 m/s which allows to load efficiently our magneto-optical trap. Together with the new (recirculating) oven, we have thus implemented an outstanding atomic source to inject the magnetic guide. Compared with the old setup, this makes the current status of the atom laser experiment very promising. Indeed, evidence for collisions between the atoms in the guide has been detected recently.

A Particle flux and mean velocity of an atomic beam

A.1 Flux out of an oven

Consider a thermal gas with density n and temperature T contained in a box with a round aperture of area A (Fig. A.1 (a)). Here we treat the case where the mean free path of the atoms is much bigger than the size of the aperture (effusive regime). The number of particles per unit time passing through the aperture is then given by

$$\Phi_0 = A \int_{v_z>0} d^3v v_z f(\boldsymbol{v}) \tag{A.1}$$

where

$$f(\boldsymbol{v}) = n \left(\frac{m}{2\pi k_B T} \right)^{3/2} \exp\left(-\frac{m\boldsymbol{v}^2}{2k_B T} \right) \tag{A.2}$$

is the Maxwell-Boltzmann velocity distribution [22] with the normalization $\int d^3v f(\boldsymbol{v}) = n$. Note that for the velocity component in the z direction, perpendicular to A, we have the condition $v_z > 0$ since only those particles pass through the hole. The straightforward calculation of the integral gives

$$\Phi_0 = \frac{1}{4} n A \bar{v}, \tag{A.3}$$

where $\bar{v} = \langle v \rangle = \frac{\int d^3v f(\boldsymbol{v}) v}{\int d^3v f(\boldsymbol{v})} = \sqrt{\frac{8k_B T}{\pi m}}$ is the average velocity of the 3D Boltzmann gas.

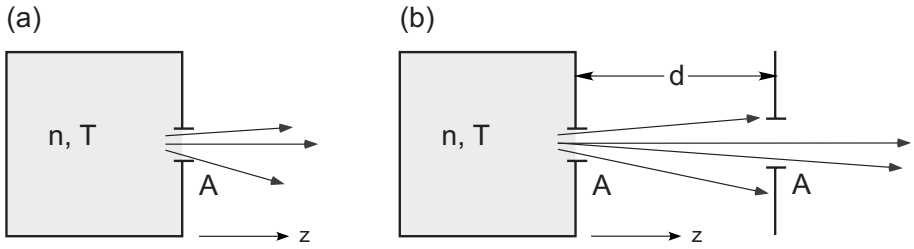

Figure A.1: *Atoms (a) coming out of an oven, and (b) after collimation.*

A.2 Flux of a collimated beam

We now calculate the flux of the collimated atomic beam. The additional round aperture A' (Fig. A.1 (b)) will reduce the flux obtained in the previous paragraph.

The transverse velocity components (parallel to the area A') are limited by the condition $v_\perp/v_z < (A'/\pi d^2)^{1/2}$, where d is the distance between the apertures A and A'. We thus calculate the integral

$$\Phi_c = A \int_{v_z>0, v_\perp<v_z(\frac{A'}{\pi d^2})^{\frac{1}{2}}} d^3v v_z f(\boldsymbol{v}) = \frac{1}{4} nA \frac{A'}{A' + \pi d^2} \bar{v}. \tag{A.4}$$

Since $A' \ll \pi d^2$ the flux of the atomic beam after collimation reads

$$\Phi_c \approx \frac{nAA'\bar{v}}{4\pi d^2}. \tag{A.5}$$

A.3 Mean velocity of an atomic beam

Whereas the number of particles contained in a box is conserved, in the case of a beam it depends linearly on time. Consider a collimated particle beam as in the previous paragraph. The number of particles having a velocity between v_z and $v_z + dv_z$ in the beam at a time t (at $t = 0$ the aperture A is opened) is given by

$$dN = Av_z t f(v_z) dv_z, \tag{A.6}$$

where $f(v_z)$ is the Maxwell-Boltzmann distribution $f(\boldsymbol{v})$ integrated over the transverse velocity components $v_\perp$ as above. The average velocity in the direction of the beam z is thus calculated as

$$\bar{v}_z^{jet} \equiv \langle v_z \rangle^{jet} = \frac{\int_0^\infty dN v_z}{\int_0^\infty dN} = \frac{\int_0^\infty dv_z f(v_z) v_z^2}{\int_0^\infty dv_z f(v_z) v_z}. \tag{A.7}$$

Applying again the approximation $A' \ll \pi d^2$ one receives

$$\bar{v}_z^{jet} \approx \sqrt{\frac{9\pi k_B T}{8m}}. \tag{A.8}$$

We also calculate the standard deviation from this mean value,

$$\Delta v_z^{jet} = \sqrt{\langle v_z^2 \rangle^{jet} - (\langle v_z \rangle^{jet})^2} = \Delta v_z^{jet} \approx \sqrt{\frac{2k_B T}{m} \left(2 - \frac{9}{16}\pi\right)}. \tag{A.9}$$

Note that in the above approximation one finds the dependence $f(v_z) \propto v_z^2 \exp(-\frac{mv_z^2}{2k_B T})$ for the longitudinal velocity distribution. In general, the mean value of a quantity $B(v_z)$ depending only on the longitudinal velocity component is thus simply calculated as

$$\langle B(v_z) \rangle = \frac{\int_0^\infty dv_z B(v_z) f(v_z) v_z}{\int_0^\infty dv_z f(v_z) v_z} = \frac{\int_0^\infty dv_z B(v_z) v_z^3 \exp(-\frac{mv_z^2}{2k_B T})}{\int_0^\infty dv_z v_z^3 \exp(-\frac{mv_z^2}{2k_B T})}. \tag{A.10}$$

References

[1] A. P. Chikkatur et al., Science **296**, 2193-2195 (2002).

[2] E. Mandonnet et al., Eur. Phys. J. D **10**, 9-18 (2000).

[3] E. L. Raab et al., Phys. Rev. Lett. **59**, 2631 (1987).

[4] P. Cren et al. Eur., Phys. J. D **20**, 107-116 (2002).

[5] W. D. Phillips, J. V. Prodan, H. J. Metcalf, J. Opt. Soc. Am. B**2**, 11 (1985).

[6] A. Scholz et al., Opt. Comm. **111**, 155-162 (1994).

[7] W. Ertmer et al., Phys. Rev. Lett. **54**, 996-999 (1985).

[8] J. Hoffnagle. Opt. Lett. **13**, 92 (1988).

[9] M. Zhu et al., Phys. Rev. Lett. **67**, 46-49 (1991).

[10] H. J. Metcalf, P. van der Straaten, *Laser Cooling and Trapping.* Springer 1999.

[11] M. A. Joffe et al., J. Opt. Soc. Am. B **10**, 12 (1993).

[12] B. H. Bransden, C.J. Joachain, *Physics of Atoms and Molecules.* Prentice Hall, second edition.

[13] R. J. Napolitano et al. Opt. Comm. **80**, 110 (1990).

[14] W. D. Phillips, H. Metcalf. Phys. Rev. Lett. **48**, 9 (1982).

[15] T. E. Barrett et al., Phys. Rev. Lett. **67**, 25 (1991).

[16] J. D. Jackson, *Classical Electrodynamics.* Wiley, third edition, 1998.

[17] P. A Molenaar et al., Phys. Rev. A **55**, 605 (1997).

[18] L. Vestergaard Hau, J. A. Golovchenko, Rev. Sci. Instrum. **65** , 12 (1994).

[19] M. R. Walkiewicz et al., Rev. Sci. Instrum. **71**, 3342 (2000).

[20] *Handbook of Chemistry and Physics.* CRC Press, 84th edition, 2003-2004.

[21] W. Demtröder.*Laserspektroskopie, Grundlagen und Techniken.* Springer, 4. Auflage, 2000.

[22] K. Huang, *Statistical Mechanics.* Wiley, second edition, 1987.

Acknowledgement

The work presented in this report was part of the first year of my PhD thesis. I had the great opportunity to spend that time in Jean Dalibard's and David Guéry-Odelin's group in Paris. I am very grateful to Jean and David for having made possible my stay in the Laboratoire Kastler-Brossel. It was a great scientific experience in a very friendly athmosphere. Also, David was so kind to read this report carefully.

Furthermore, I'd like to thank Thierry Lahaye, the other PhD student of the group. His careful working style is amazing. Thanks also go to Johnny Vogels who helped me in the careful design and the realization of the Zeeman slower. Also involved in the practical work was Leticia Tarruel whom I'd like to thank for her assistance during her internship.

My work was supported by a Marie-Curie Fellowship (QPAF).